Proceedings of the 21st ICSMGE, Vienna, Austria, 14 – 19 June 2026. Pistrol, Adam & Schweiger (eds.)
Published by: ÖGG, Austrian Society for Geomechanics, Salzburg, Austria, ISBN 978-3-9503898-4-5
https://doi.org/10.53243/ICSMGE2026-465

Drying effect on the microstructure of lime-treated saline soil

Cen Gao[1,2], Yujun Cui[1]
1 : École nationale des ponts et chaussées, Laboratoire Navier/CERMES, 6 – 8 av. Blaise Pascal, Cité Descartes, Champs-sur-Marne, 77455 Marne-la-Vallée cedex,France. cen.gao@enpc.fr

Nadia Benahmed[2], Sylvie Nicaise[2]
2 : INRAE, Aix Marseille Univ, RECOVER, Equipe G2DR, 3275 route Cézanne, CS 40061, 13182 Aix-en-Provence, France.

ABSTRACT: Lime treatment is considered as an effective method to enhance the mechanical performance and durability of natural soils. In this study, the effect of drying on the microstructure evolution of lime-treated silty soils with different salinities was investigated through mercury intrusion porosimetry (MIP). Although the overall void ratio of soil specimens remains almost constant upon drying, the pore size distribution (PSD) changes significantly. Specifically, the clay fraction coating the soil skeleton was found to shrink, leading to the development of nano-fissures. The pore size distribution of the studied lime-treated silty soil transitions from a bi-modal to a tri-modal pattern as the water content decreases to approximately 8% and eventually reverts to a bi-modal distribution upon further drying to a water content of 3%. This evolution is due to the combined effects of nano-fissures formation and pores enlargement throughout the drying process. It can be inferred that soils with higher salinity exhibit greater microstructure stability likely due to the enhanced formation of cementitious compounds under higher ion concentration. By categorizing the pores into inter-aggregate pores and intra-aggregate pores, it is observed that drying process induces an increase of the proportions of inter-aggregate pores. These findings contribute to a deeper understanding of the microstructural evolution of lime-treated soils servicing in saline environments.

KEYWORDS: lime-treated soil, soil salinity, pore size distribution, drying effect.

1 INTRODUCTION

Saline soils are widely distributed in marine areas and arid regions, and show undesirable engineering properties and complex geotechnical behaviors (Li et al. 2016a; Liu et al. 2016). The presence of salt ions enhances the electrostatic screening effect of the clay particle's negative charge. This expels the diffused layer water and induces the compression of diffused double layer in clay minerals, leading to the decrease of repulsive force between soil particles and promoting particle aggregation and flocculation (Mitchell & Soga 2005; Ying et al. 2021a). These microstructure variations, in turn, influence the macroscopic behaviors of saline soils. With increasing salinity, the liquid limit and optimum water content of highly plastic soils decrease due to both a compression of diffused double layer and a more oriented face-to-face clay particles arrangement (Sridharan et al. 2002; Horpibulsuk et al. 2011; Durotoye et al. 2016; Cui et al. 2025). Numerous studies reported geotechnical failures in saline soil constructions, including differential settlement, salt swelling, and salt-induced erosion (Rajasekaran & Rao, 2002; Feng et al., 2022).

Lime treatment is a widely adopted technique to improve soil mechanical performance and durability through a series of physico-chemical reactions (Locat et al. 1990; Vitale et al. 2017; Wang et al. 2017). After lime addition, hydration and cation exchange happened rapidly, leading to particles flocculation and thus resulting in the early improvement of soil strength (Bell, 1996). Subsequently, the pozzolanic reaction occurred, forming the cementitious compounds and enhancing the bonds between soil particles (Al-Mukhtar et al. 2012; Tang et al. 2011). Ying et al. (2021a, 2022) reported that lime-treated saline soils exhibited higher small strain shear modulus and compressive modulus than untreated soils. It is widely admitted that lime treatment technique effectively enhances the unconfined compressive strength and shear strength of soils by cementing soil aggregates and reinforcing soil structures (Al-Mukhtar et al. 2010; Wang et al. 2020).

Exposure to atmospheric conditions inevitably leads to soil drying, which causes clay shrinkage, fissures development and soil structure degradation (Tang et al., 2012). For lime treated soils, Nabil et al. (2018) pointed out that the soils showed reduced shrinkage potential during the drying process, in contrast to the widely observed volume shrinkage in untreated soils (Romero, 2013). The formed cementitious compounds connect the adjacent soil particles and enhance the structural stability of soil aggregates, limiting the clay shrinkage and fissures development (Poncelet & François 2019). However, Stoltz et al. (2012) observed obvious volumetric changes in lime-treated soils during drying, characterized by shrinkage in both macro-pores and micro-pores. These contrasting observations highlight the importance to clarify the microstructure evolution of lime-treated soils during drying for the long-term assessment of constructions.

In this study, the microstructure evolution of lime-treated saline soils during drying was investigated using mercury intrusion porosimetry (MIP) technique. Three salinities levels, 0.00‰, 2.10‰, and 6.76‰, were selected to prepare specimens, corresponding to non-salted soil, soil salinity on site and seawater salinity, respectively. The experimental results obtained were analyzed to clarify the pore structure variations of lime-treated saline soils occurring during the drying process.

2 MATERIALS AND METHODS

Soils used in this study were collected from Les Salins de Giraud in southern France, which is classified as sandy silt (ASTM D2487-17, 2017) based on the geotechnical properties presented in Table 1. The grain size distribution of tested soil is shown in Figure 1. Mineralogical analysis showed that the soil contained 34% calcite, 29% quartz, 9% feldspar, and 28% clay minerals. The clay fraction comprised 14% chlorite, 12% illite and 2% kaolinite (Figure 2).

Table 1. Geotechnical properties of the tested soil.

Property	Value
Liquid limit, w_L (%)	29.7
Plastic limit, w_p (%)	23.2
Plasticity index, *PI*	6.5

Specific gravity, G_s	2.71
Specific surface area (m^2/g)	24.0

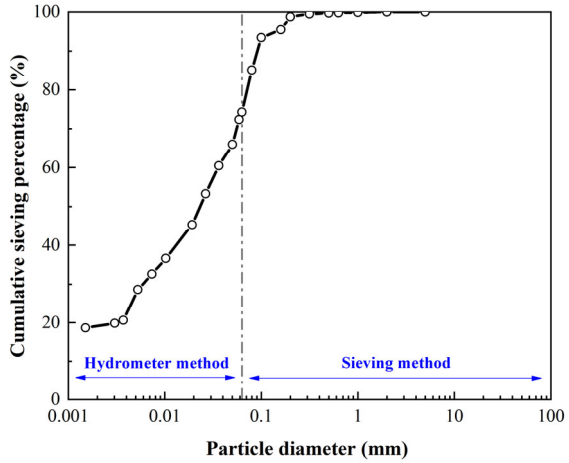

Figure 1. Particle size distribution curve of studied soil.

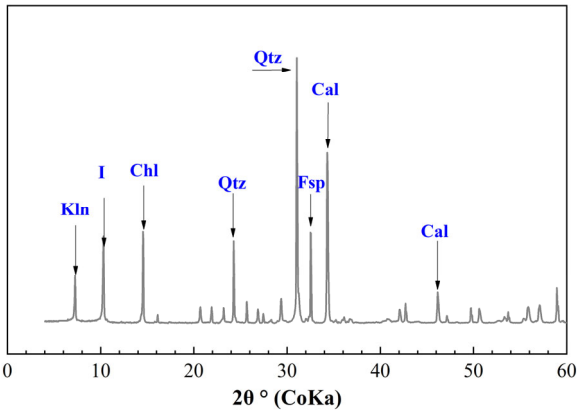

Figure 2. X-ray diffraction result of studied soil (Kln: kaolinite; I: illite; Chl: chlorite; Qtz: quartz; Fsp: feldspar; Cal: calcite).

Quicklime with CaO content higher than 90% was used in this study. Based on the pH of lime-soil-water mixture solution (ASTM D6267-19, 2019), 2% lime dosage was considered as the optimum lime content and was used for the experimental tests (Figure 3).

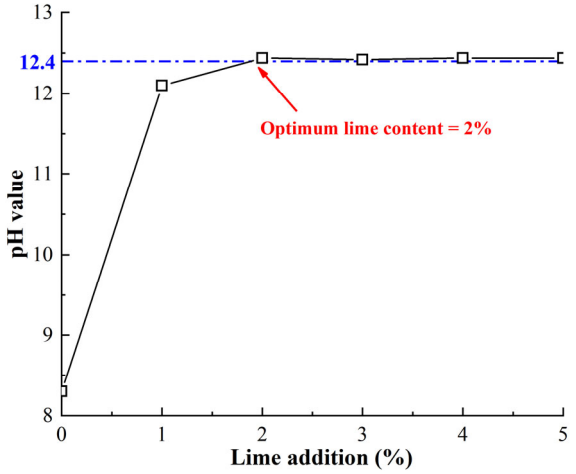

Figure 3. pH values of lime-soil-water mixtures with different lime dosages.

To prepare the salted soil specimens, synthetic salty water with different salinities was formulated based on the French standard (AFNOR NF P 18-837, 1993), which mainly contains Cl^-, Na^+, K^+, Ca^{2+} and Mg^{2+} (Table 2). A total of 3 different salinities were used, namely 0.00‰, 2.10‰ (representing in situ soil salinity), and 6.76‰ (equivalent to seawater salinity). The preparation of salted soil followed the procedures outlined in Ying et al. (2021c).

Table 2. Salt composition of synthetic sea water.

Salts	Concentration (g/L)
NaCl	30.0
$MgCl_2.6H_2O$	6.0
$MgSO_4.7H_2O$	5.0
$CaSO_4.2H_2O$	1.5
$KHCO_3$	0.2

The soil taken from the site was firstly cleaned by removing gravels and roots, then sieved through 0.4 mm sieve. Subsequently, the soil was mixed with dry lime and then wet by corresponding saline water. According to the Proctor compaction curve of the untreated soil (Figure 4), all the specimens were statistically compacted to a dry density of 1.63 Mg/m^3, at a water content of 19%. The compacted specimens were then cured for 90 days prior to testing.

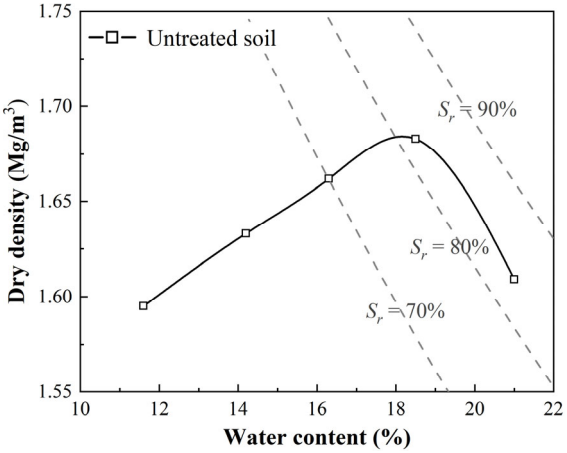

Figure 4. Normal Proctor curve of studied soil.

During the test, the specimens were firstly saturated and then air-dried under controlled laboratory conditions (20 ± 2°C temperature and 50 ± 5% relative humidity). Once the specimens reached the target water content, small samples were taken from the central part of the specimen, frozen and lyophilized, then used for the MIP tests to investigate the microstructure. An Autopore V 9600 mercury intrusion porosimeter was used, applying pressure ranging from 3.6 kPa to 230 MPa, which corresponds to the pore diameter varied from 0.006 μm to 350 μm.

3 RESULTS

3.1 *Microstructure evolution during saturation*

The pore size density functions curves and cumulative mercury intrusion curves of specimens with different salinities are presented in Figure 5. It appears from Figure 5(a) that the specimens exhibit a similar bi-modal pore distribution after 90-day of curing. With increasing salinity, the frequency of intra-aggregate pores increases, while their pore diameter slightly decreases. All specimens show similar frequency and diameter in inter-aggregate pores. After saturation, although the specimens kept a bi-modal pore size distribution, the changes in pore structure differed among soils under different salinities.

For the non-saline soil (0.00‰), a distinct contraction trend between the two pore peaks was observed after saturation (Figure 5(b)). The diameter of inter-aggregate pores decreased from approximately 10.1 μm to 7.0 μm, while that of intra-

aggregate pores increased from 1.1 μm to 1.9 μm. A similar contraction trend was also observed in soils with 2.1‰ and 6.76‰ salinity, while the variation range decreased with increasing salinity. Moreover, the frequency of inter-aggregate pores is decreased after saturation, with the most pronounced reduction observed in the soil with 6.76‰ salinity. The cumulative mercury intrusion curves in Fig. 5(c) shows that the non-saline specimens exhibited the highest mercury intrusion void ratio among all specimens after curing. After saturation, the total void ratio of all specimens decreased and reached a similar value.

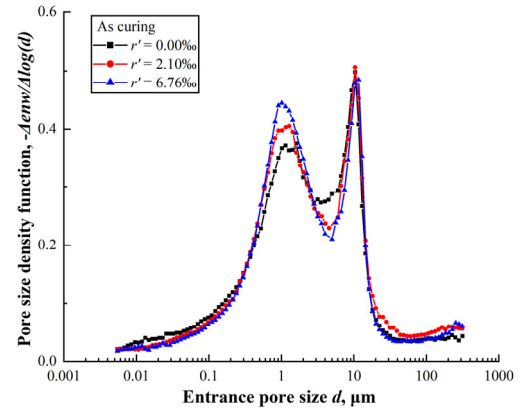

(a)

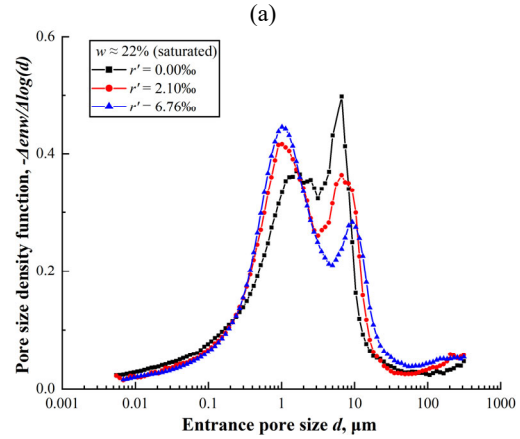

(b)

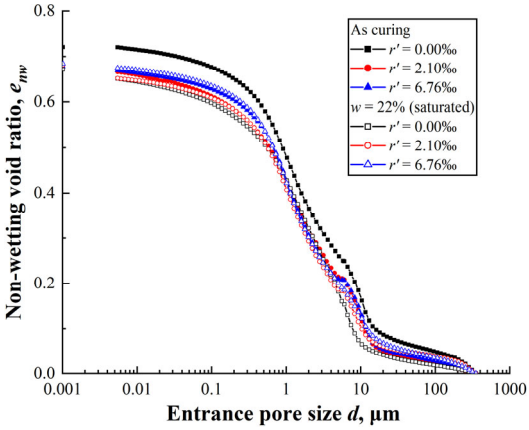

(c)

Figure 5. Pore size density (PSD) curves and cumulative mercury intrusion curves of specimens with different salinities: (a) PSD curves (as curing); (b) PSD curves (saturated); (c) cumulative mercury intrusion curves (as curing and saturated).

3.2 *Microstructure evolution during drying*

Figures 6 and 7 depict the pore size density function curves and cumulative mercury intrusion curves for specimens at five water contents: around 22% (saturated), 17%, 11%, 8%, and 3%. At the beginning of drying (22% water content), all specimens show a bi-modal pore size distribution, with two populations of inter-aggregate pores and intra-aggregate pores.

For the soil with 0.00‰ salinity, the diameter and frequency of inter-aggregate pores gradually increase, while the diameter of intra-aggregate pores gradually decreases as the water content decreases from 22.3% to 10.9%. Similar variation is observed for the soil with 2.10‰ salinity. In contrast, for the soil with 6.76‰ salinity, only the frequency of inter-aggregate pores increases while their pore size keeps almost constant during drying. When the water content decreased to around 8%, the pore distribution of all specimens changed from bi-modal to tri-modal distribution, with an appearance of a nano-pores peak. With further drying to 3% water content, this tri-modal distribution changed to bi-modal pattern. As the water content decreased from 11% to 3%, the size of inter-aggregate pores almost kept constant at around 10 μm, with a slight increase in the frequency. A slightly size decreasing for the soils with 6.76‰ salinity can be observed from 8% to 3% water content, which may be attributed to the salt crystallization. It should be noted that the initial void ratio shows negligible variation during the drying process. The slight differences in intruded mercury ratio may be attributed to heterogeneity of the specimens (Delage et al., 1996).

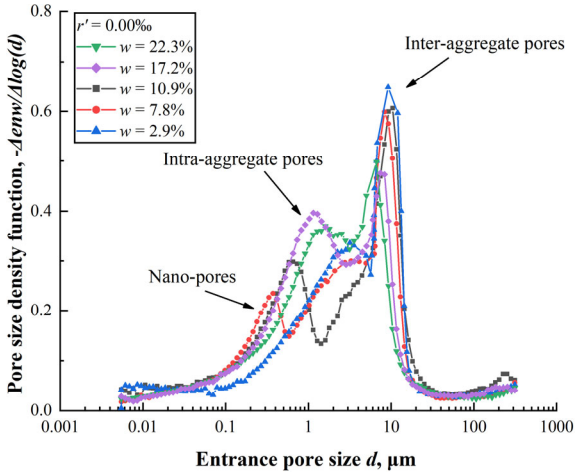

(a)

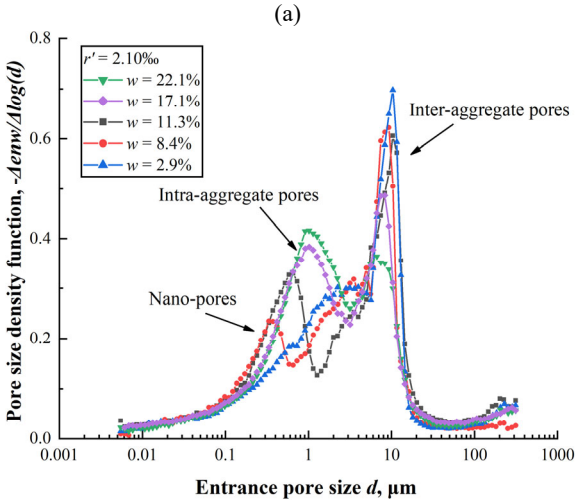

(b)

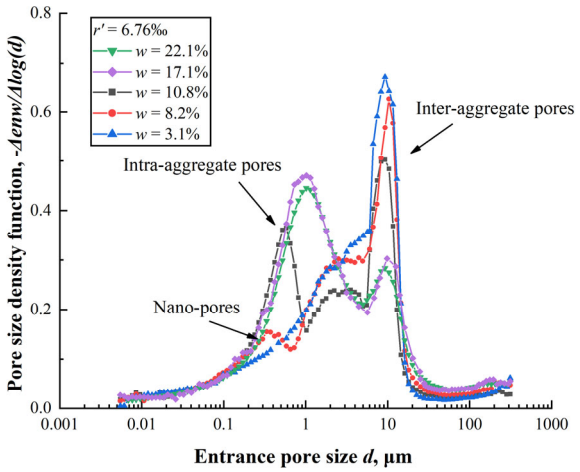

(c)

Figure 6. Pore size density curves of specimens during drying: (a) r' = 0.00‰; (b) r' = 2.10‰; (c) r' = 6.76‰.

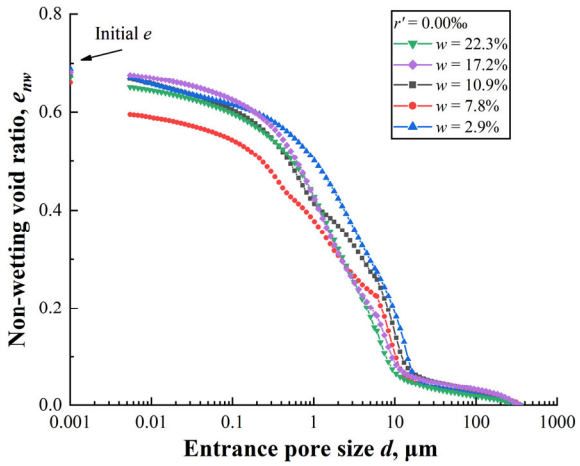

(a)

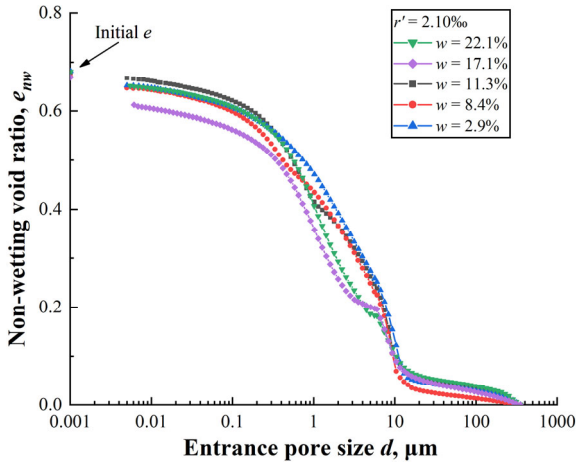

(b)

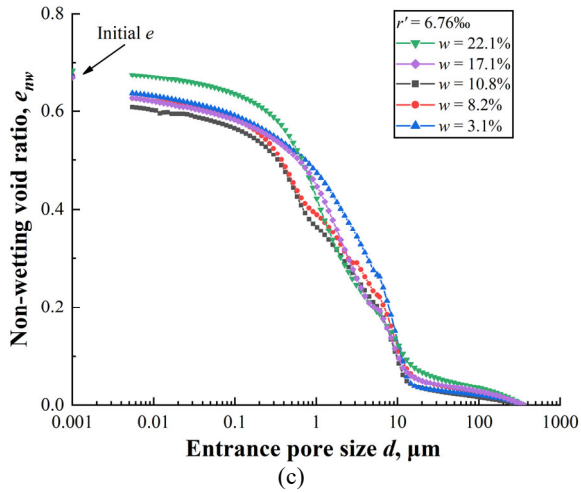

(c)

Figure 7. Cumulative mercury intrusion curves of specimens during drying: (a) r' = 0.00‰; (b) r' = 2.10‰; (c) r' = 6.76‰.

The proportions of inter-aggregate pores and intra-aggregate pores were calculated based on the intruded mercury volume data from MIP tests and are shown in Figure 8. A threshold pore diameter to distinguish these two kinds of pores is set as 5.0 μm. Overall, the proportion of inter-aggregate pores increases while that of intra-aggregate pores decreases during the drying process. At the saturation stage, the proportion of inter-aggregate pores is obviously higher than that of intra-aggregate pores, with around 70% intra-aggregate pores and 30% inter-aggregate pores. As drying progresses, the difference between the proportions of inter-aggregate pores and intra-aggregate pores decreases. By the time the water content decreases to 3%, the proportion of inter-aggregate pores exceeds 40% for all salinities. For the soils with 0.00‰ and 2.10‰ salinities, a reduction of inter-aggregate pores occurred between 11% to 8% water content, which may be attributed to the formation of large quantities of dry-induced fissures (nano-pores).

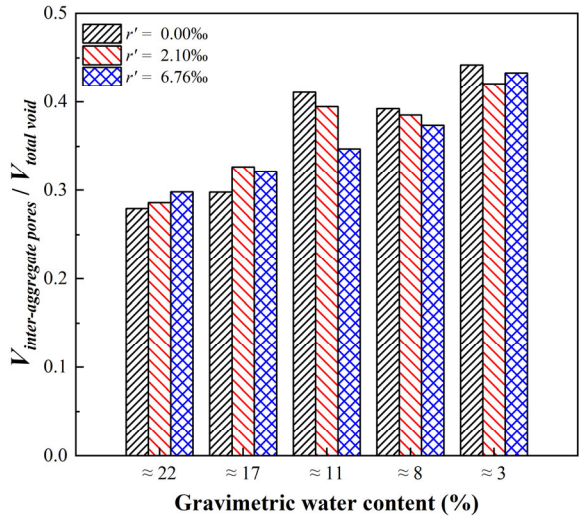

(a)

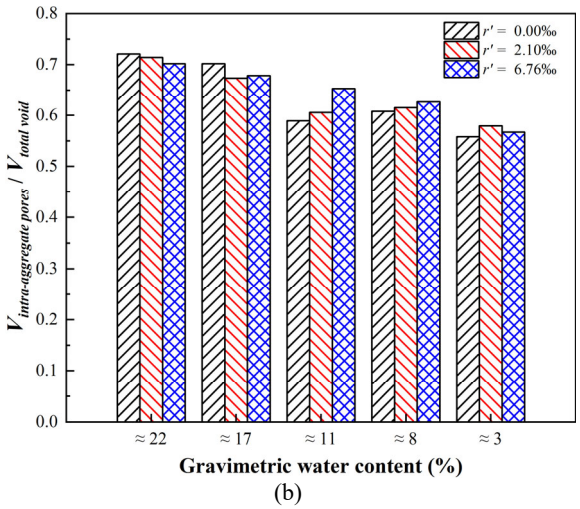

(b)

Figure 8. Proportions of inter-aggregate pores and intra-aggregate pores during drying: (a) inter-aggregate pores; (b) intra-aggregate pores.

4 DISCUSSIONS

The PSD curves in Figure 5(a) showed that the frequency of intra-aggregate pores increased while their diameter slightly decreased with increasing salinity. This trend indicates a more complicated and densified pore structure in salted specimens. In synthetic seawater, salt ions (Na^+, K^+, etc.) promote ions transfer and ion exchange activities, which facilitates the pozzolanic reaction and promotes the formation of cementitious compounds (Koslanant et al., 2006). These cementitious compounds form at the contact between soil particles, strengthening the particle connection and bonding, resulting in a larger amount of intra-aggregate pores in salted specimens. Compared to the variations in intra-aggregate pores, the inter-aggregate pores of specimens with different salinities exhibited similar frequency and size. Shi and Zhao (2020) pointed out that the behavior of soils with low clay fraction was mainly governed by the soil skeleton, i.e. silt/sand grains rather than the clay content. Since in lime treatment, the main process is related to the ions reaction between clay minerals and added lime, the inter-aggregate pores distributions, which is dominated by silt/sand skeleton, are similar in soils with different salinities. During the saturation process, clay particles absorbed the water and underwent swelling, leading to a decrease in the diameter of inter-aggregate pores. Additionally, the reduction of matric suction changes the soil structures, resulting in the collapse of initial larger pores and formation of more small pores (Li et al., 2016b; Xie et al., 2018). Thus, the two peaks observed in pore size distribution curves exhibit a contraction trend, especially in non-saline specimens. As more formed cementitious compounds in salted environment further improve the stability of pore structures, the contraction tendency decreased with increasing salinity during saturation.

The MIP results during the drying process showed that the PSD significantly changed while the total void ratio remained almost constant across all specimens with different salinities. This observation can be attributed to the shrinkage of the clay fraction coating on the soil skeleton and the stability of the silt/sand skeleton in the tested soil (Ying et al., 2021b). During the drying process, clay fraction in the soil shrinks and enlarges the pores between soil aggregates. This is evidenced by the increase of the frequency and the diameter of inter-aggregate pores from 22% to 11% water content, especially in the soils with 0.00‰ and 2.10‰ (Figure 6(a)(b)). Meanwhile, the soil aggregates contract under the higher matric suction, leading to a reduction of the size of intra-aggregate pores (Figure 6). The soil shrinkage leads to the occurrence of micro-fissures within the clay fraction and at the interface between the clay particles and the soil skeleton (Tang et al., 2011; Sun and Cui, 2018). Further drying to 8% water content, the nano-fissures developed and formed a new nano-pores peak, resulting in the increasing proportion of intra-aggregate pores (Figure 8). However, it was observed that fewer nano-pores were formed in 6.76‰ salinity soils (Figure 6), which may be attributed to the reinforcement effect of more cementitious compounds formed in that soils. Similar appearance of nano-pores has been reported by Sun and Cui (2018) and Ying et al. (2021b) on untreated silty soils. Due to the low clay content and activity of studied silty soil, the pozzolanic reactions were relatively limited, leading to the formation of amorphous cementitious phases (Ying et al. 2020), which were less effective in controlling fissures development. When the water content reached 3%, the PSD of all specimens reverted to a bi-modal distribution. The nano-fissures formed previously were further enlarged into the intra-aggregate pores, increasing their frequency. Meanwhile, the frequency of inter-aggregate pores slightly increased due to the enlargement of intra-aggregate pores. It can be found that in soil with 6.76‰ salinity, the diameter of inter-aggregate pores slightly decreased between 8% and 3% water content, which may be attributed to the salt crystallization (Espinosa et al., 2008; Xiong et al., 2025).

5 CONCLUSIONS

In this study, the drying effect on the microstructure evolution of lime-treated saline soils was investigated using MIP technique. The results revealed that the total void ratio exhibited neglectable variations during the drying process, while the pore structure distribution showed significant changes. Indeed, the later varied from bi-modal characteristics at 22% water content to tri-modal pattern with a new peak of nano-pores appearance as drying process continued to around 8% water content, and finally reverted to bi-modal distribution upon further drying to 3% water content for soils with different salinities. These variations on PSD could be attributed to the shrinkage of the clay fraction, which leads to the occurrence of nano-fissures and the further enlargement to intra-aggregate pores at 3% water content. The reduced pore structure sensitivity at higher salinity suggests improved structural stability and potentially lower shrinkage-induced deformation in lime-treated saline soils than non-saline soils. These findings indicate that salinity facilitates the maintenance of pore structure integrity in lime-treated soils during the drying process.

6 ACKNOWLEDGEMENTS

The authors would like to thank the China Scholarship Council (CSC). The supports provided by Ecole Nationale des Ponts et Chaussées (ENPC) and INRAE are also greatly acknowledged.

7 REFERENCES

AFNOR NF P 18-837. (1993). Standard for special products for hydraulic concrete construction-Hydraulic binder based needling and/or sealing products-Testing of resistance against seawater and/or water with high sulphate contents.

Al-Mukhtar, M., Lasledj, A., and Alcover, J.F. 2010. Behaviour and mineralogy changes in lime-treated expansive soil at 20◦C. *Applied Clay Science* 50, 191–198.

Al-Mukhtar, M., Khattab, S., and Alcover, J.F. 2012. Microstructure and geotechnical properties of lime-treated expansive clayey soil. *Engineering Geology* 139/140, 17–27.

ASTM D2487-17 2017. Standard Practice for Classification of Soils for Engineering Purposes (Unified Soil Classification System). West Conshohocken, PA.

ASTM D6276-19 2019. Standard Test Method for Using pH to Estimate the Soil-lime Proportion Requirement for Soil Stabilization. (Unified Soil Classification System). West Conshohocken, PA.

Bell, F.G. 1996. Lime stabilization of clay minerals and soils. *Engineering Geology* 42, 223–237.

Cui, L.Y., Ye, W.M., Wang, Q., Chen, Y.G., Chen, B., and Cui, Y.J. 2025. Experimental investigation on swelling and gas breakthrough properties of GMZ bentonite considering alkaline solution effects. *Engineering Geology* 107933.

Delage, P., Audiguier, M., Cui, Y.J. and Howat, M.D. 1996. Microstructure of a compacted silt. *Canadian Geotechnical Journal* 33(1), 150-158.

Durotoye, T.O., Akinmusuru, J.O., Ogbiye, A.S., and Bamigboye, G.O. 2016. Effect of common salt on the engineering properties of expansive soil. *International Journal of Engineering and Technology* 6(7), 233-241.

Espinosa, R. M., Franke, L., and Deckelmann, G. 2008. Phase changes of salts in porous materials: Crystallization, hydration and deliquescence. *Construction and Building Materials* 22(8), 1758-1773.

Feng, B., Wang, H., Li, S., Ji, K., Li, L., and Xiong, R. 2022. The durability of asphalt mixture with the action of salt erosion: A review. *Construction and Building Materials* 315, 125749.

Horpibulsuk, S., Yangsukkaseam, N., Chinkulkijniwat, A., and Du, Y.J. 2011. Compressibility and permeability of Bangkok clay compared with kaolinite and bentonite. *Applied Clay Science* 52, 150-159.

Koslanant, S., Onitsuka, K., and Negami, T. 2006. Influence of salt additive in lime stabilization on organic clay. *Geotechnical Engineering* 37(2), 95.

Li, M., Chai, S.X., Du, H.P., and Wang, C. 2016a. Effect of chlorine salt on the physical and mechanical properties of inshore saline soil treated with lime. *Soils and Foundations* 56, 327-335.

Li, P., Vanapalli, S., and Li, T. 2016b. Review of collapse triggering mechanism of collapsible soils due to wetting. *Journal of Rock Mechanics and Geotechnical Engineering* 8(2), 256-274.

Liu, X.F., de Carteret, R., Buzzi, O.P., and Fityus, S.G. 2016. Microstructural effects of environmental salinity on unbound granular road pavement material upon drying. *Acta Geotechnica* 11, 445-451.

Locat, J., Berube, M.A., and Choquette, M. 1990. Laboratory investigations on the lime stabilization of sensitive clays: shear strength development. *Canadian Geotechnical Journal* 27, 294–304.

Mitchell, J.K., and Soga, K. 2005. *Fundamentals of soil behaviour.* 3rd edn. John Wiley &Sonc, Inc.

Nabil, M., Mustapha, A., and Rios, S. 2018. Long term evaluation of wetting-drying cycles for compacted soils treated with Lime, *In Conference of the Arabian Journal of Geosciences* (pp. 277-281).

Poncelet, N., and François, B. 2019. Desiccation crack in lime-treated silty clay: experimental evaluation and constitutive interpretation. E3S Web Conferences 92.

Rajasekaran, G., and Rao, S.N. 2002. Compressibility behaviour of lime-treated marine clay. *Ocean Engineering* 29, 545–559.

Romero, E. 2013. A microstructural insight into compacted clayey soils and their hydraulic properties. *Engineering Geology* 165, 3-19.

Shi, X.S., and Zhao, J. 2020. Practical estimation of compression behavior of clayey/silty sands using equivalent void-ratio concept. Journal of Geotechnical and Geoenvironmental Engineering 146 (6) 04020046.

Sridharan, A., El-Shafei, A., and Miura, N. 2002. Mechanisms controlling the undrained strength behavior of remolded Ariake marine clays. *Marine Georesources and Geotechnology* 20(1), 21-50.

Stoltz, G., Cuisinier, O., and Masrouri, F. 2012. Multi-scale analysis of the swelling and shrinkage of a lime-treated expansive clayey soil. *Applied Clay Science* 61, 44–51.

Sun, W.J., and Cui, Y.J. 2018. Investigating the microstructure changes for silty soil during drying. *Geotechnique* 68(4) 370–373.

Tang, C.S., Shi, B., Liu, C., Suo, W.B., and Gao, L. 2011. Experimental characterization of shrinkage and desiccation cracking in thin clay layer. *Applied Clay Science* 52 (1–2) 69–77.

Vitale, E., Deneele, D., Paris, M., and Russo, G. 2017. Multi-scale analysis and time evolution of pozzolanic activity of lime treated clays. *Applied Clay Science* 141, 36–45.

Wang, Y.J., Cui, Y.J., Tang, A.M., Benahmed, N., and Duc, M. 2017. Effects of aggregate size on the compressibility and air permeability of lime-treated fine-grained soil. *Engineering Geology* 228, 167–172.

Wang, Y.J., Cui, Y.J., Benahmed, N., Tang, A.M., and Duc, M. 2020. Changes of small strain shear modulus and suction for a lime-treated silt during curing. *Geotechnique* 70, 276–280.

Xie, W. L., Li, P., Vanapalli, S. K., and Wang, J. D. 2018. Prediction of the wetting-induced collapse behaviour using the soil-water characteristic curve. *Journal of Asian Earth Sciences* 151, 259-268.

Xiong, Q. X., Tong, L. Y., Huang, J. K., Yang, J., and Liu, Q. F. 2025. Salt crystallization in porous materials: a quasi-local transport model for evaluating pore filling process. *Construction and Building Materials* 462, 139904.

Ying, Z., Cui, Y.J., Benahmed, N., and Duc, M. 2020. Changes in mineralogy and microstructure of a lime-treated silty soil during curing time. *In E3S Web of Conferences* Vol. 195, p. 03044.

Ying, Z., Cui, Y.J., Benahmed, N., and Duc, M. 2021a. Changes of small strain shear modulus and microstructure for a lime-treated silt subjected to wetting-drying cycles. *Engineering Geology* 293, 106334.

Ying, Z., Cui, Y.J., Benahmed, N., and Duc, M. 2021b. Drying effect on the microstructure of compacted salted silt. *Geotechnique* 73(1), 62-70.

Ying, Z., Duc, M., Cui, Y.J., and Benahmed, N. 2021c. Salinity assessment for salted soil considering both dissolved and precipitated salts. *Geotechnical Testing Journal* 44(1), 130-147.

Ying, Z., Benahmed, N., Cui, Y.J., and Duc, M. 2022. Wetting-drying cycle effect on the compressibility of lime-treated soil accounting for wetting fluid nature and aggregate size. *Engineering Geology* 307, 106778.